A Porous Polycrystalline $NiCo_2P_x$ As Highly Efficient Host For Sulfur Cathode of Li-S batteries

Lu Wang[†,a] Meng Zhang,[†,a] Bo Zhang,[a] Bin Wang,[a] Jianmin Dou,[b] Zhen Kong,[a] Chunsheng Wang,[a] Xiuping Sun,[a] Yitai Qian, [a] Liqiang Xu[*a]

Contents

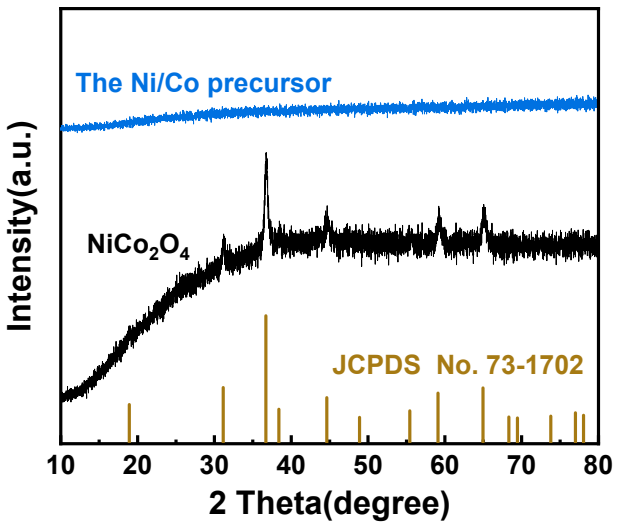

Figure S1. XRD pattern of the amorphous Ni/Co containing precursor and the derived $NiCo_2O_4$.

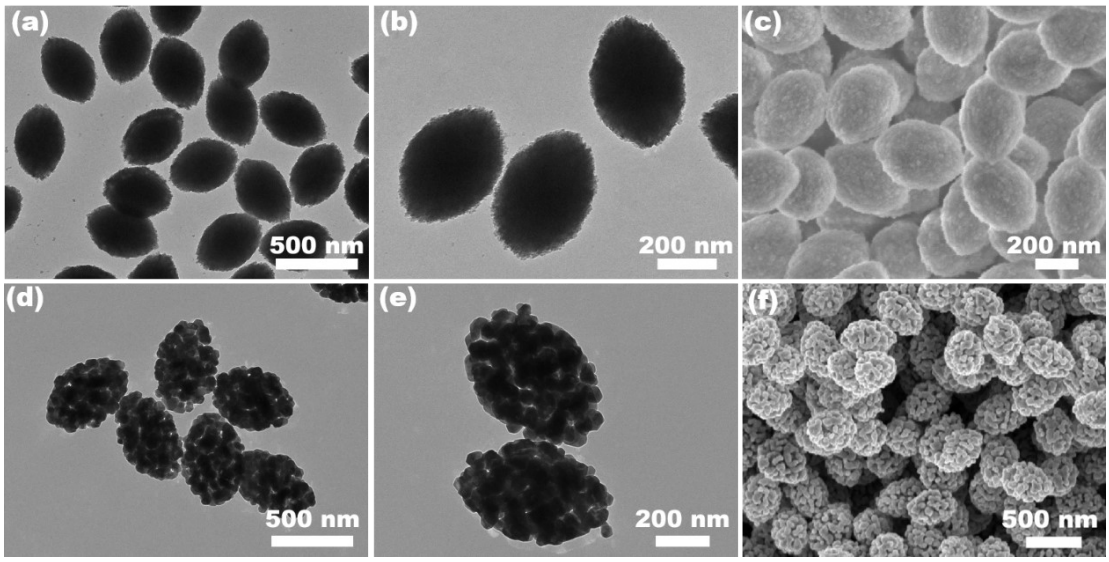

Figure S2. (a), (b) TEM images and (c) SEM image of the amorphous Ni/Co precursor; (d), (e) TEM images and (f) SEM image of the $NiCo_2O_4$.

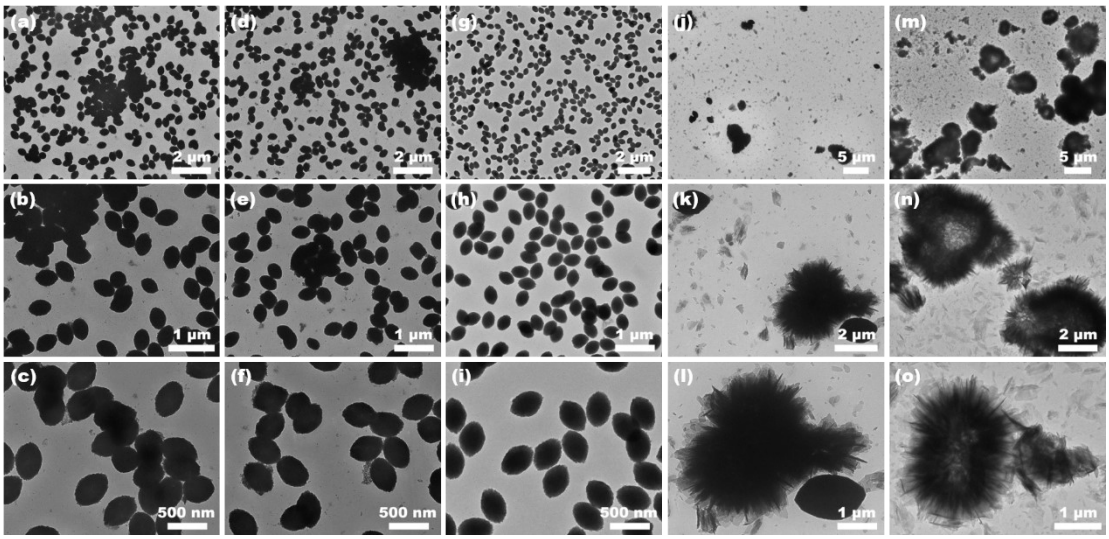

Figure S3. TEM images of amorphous Ni/Co precursor synthesized with different PVP dosage: (a)-(c) 160 mg; (d-f) 180 mg；(g-i) 200 mg；(j-l) 220 mg；(m-o) 240 mg.

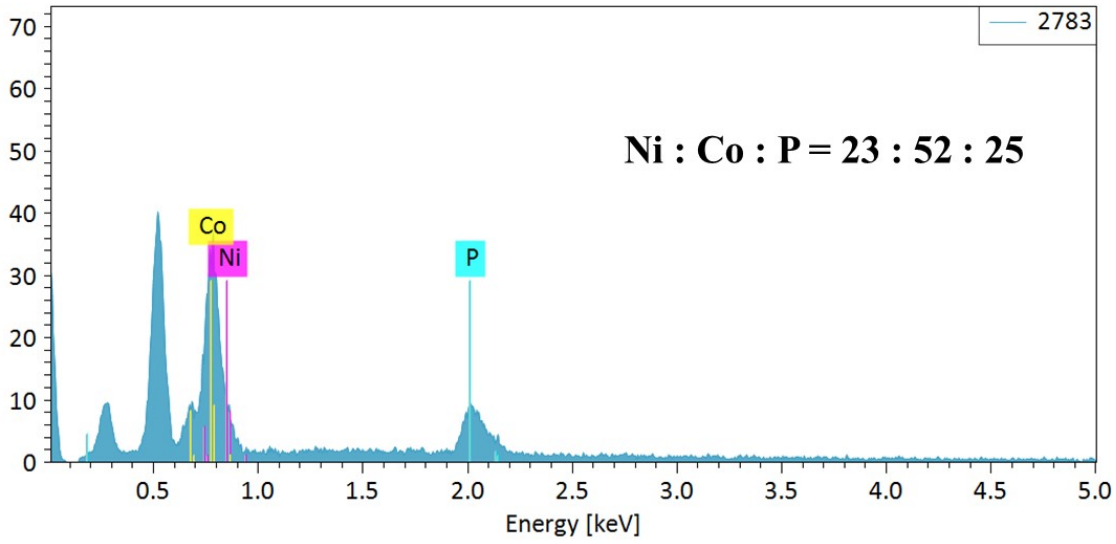

Figure S4. EDX spectrum of $NiCo_2P_x$, where content of O and P in the $NiCo_2P_x$ is 65.70 at% and 11.17 at%, respectively (with a ratio of 5.88: 1).

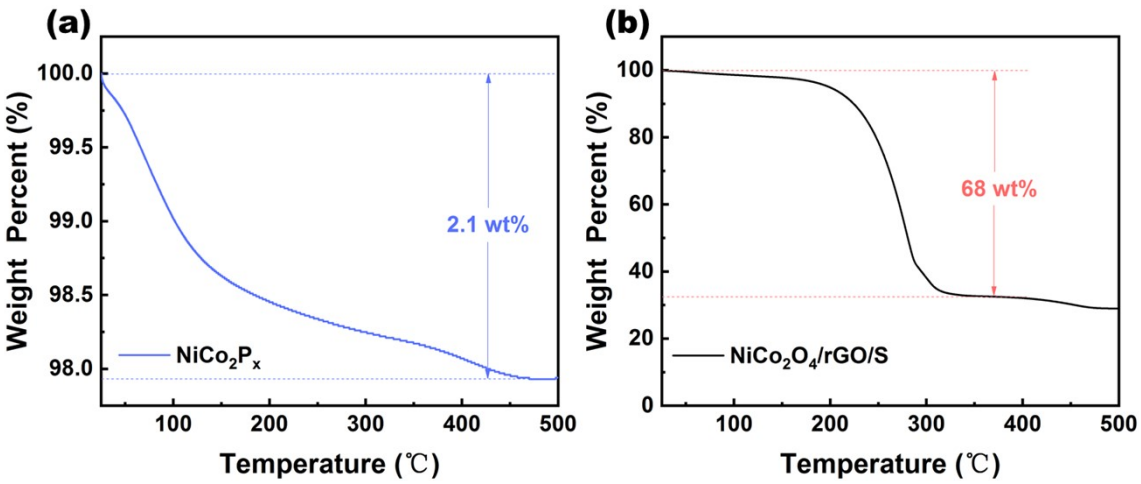

Figure S5. TGA curves of the $NiCo_2P_x$ and $NiCo_2O_4$/rGO/S composite.

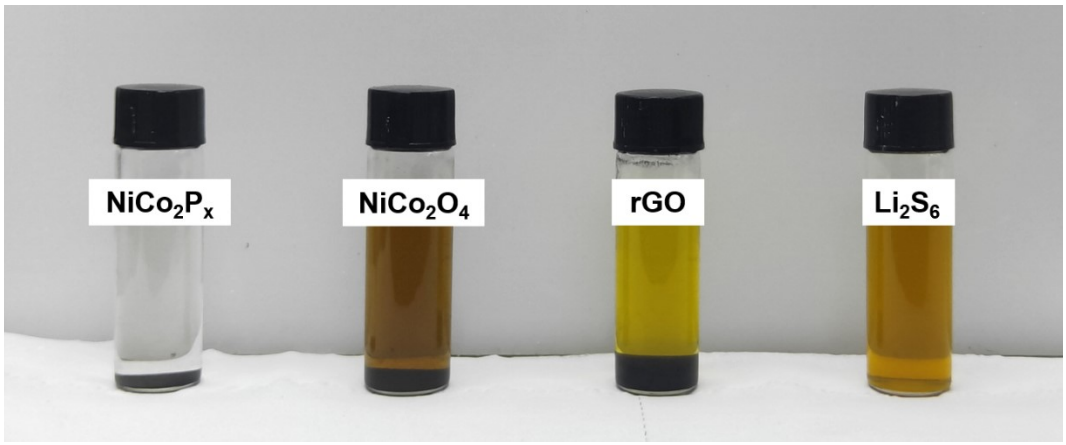

Figure S6. Color comparison among the blank Li_2S_6 solution and those soaked with $NiCo_2P_x$, $NiCo_2O_4$, and rGO.

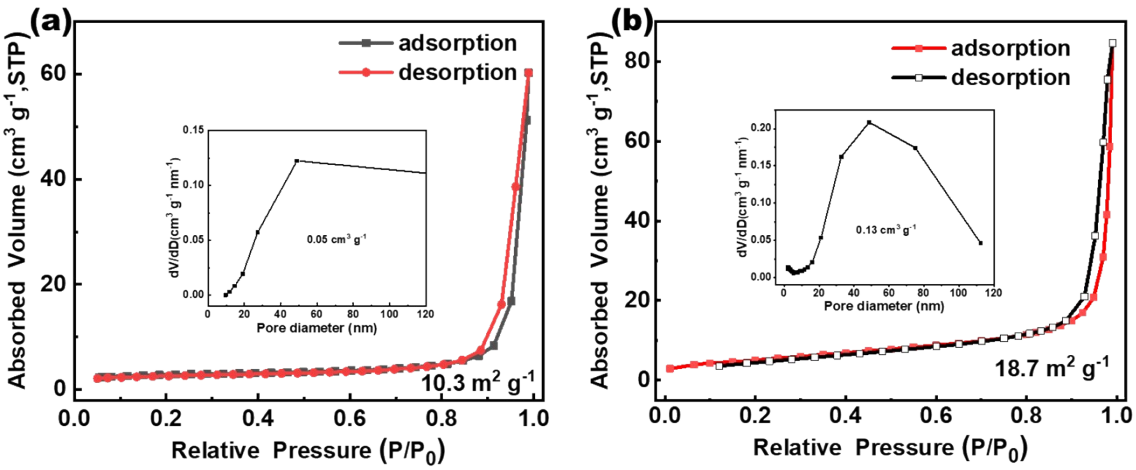

Figure S7. N_2 adsorption/desorption isotherms and their pore size distribution curves (inset) of (a) $NiCo_2O_4$ and (b) $NiCo_2P_x$.

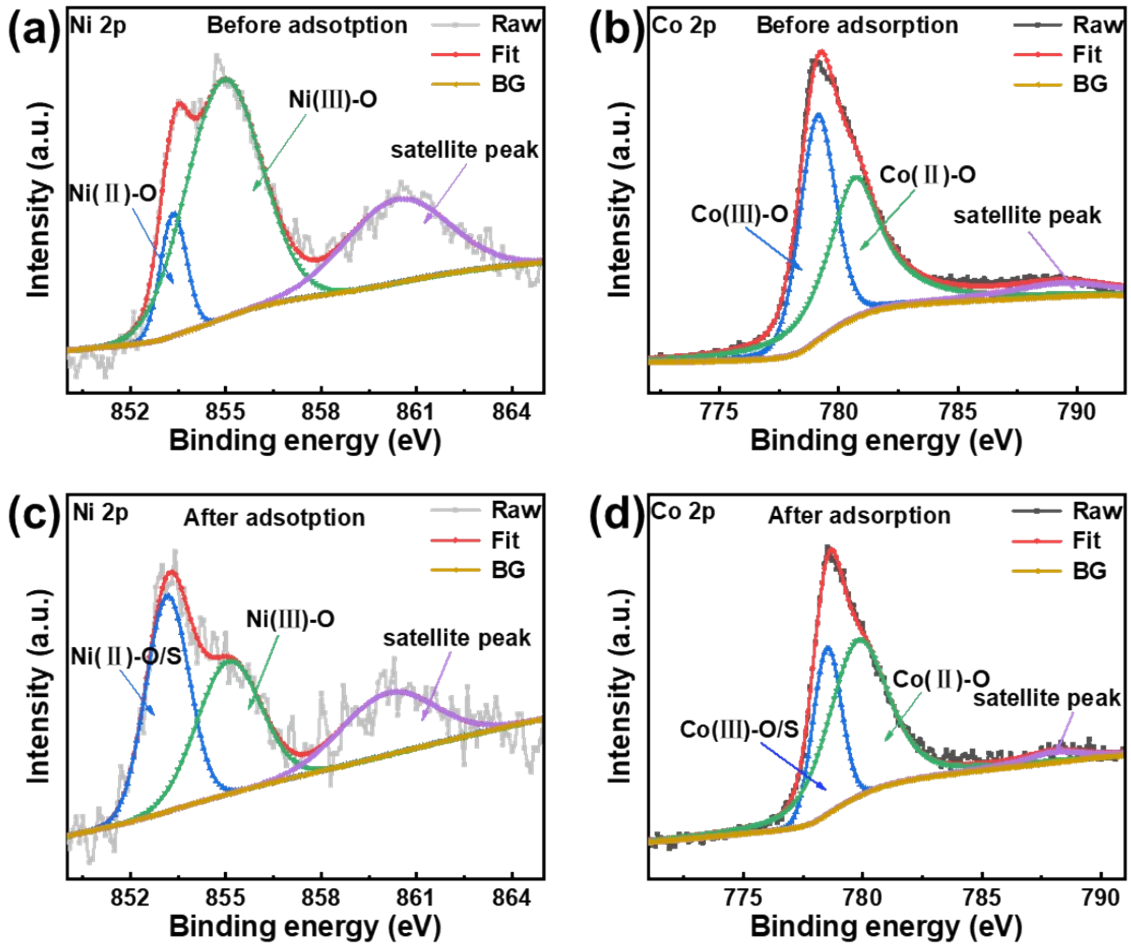

Figure S8. High resolution XPS spectra for the Ni 2p and Co 2p of $NiCo_2O_4$, before and after adsorption of Li_2S_6.

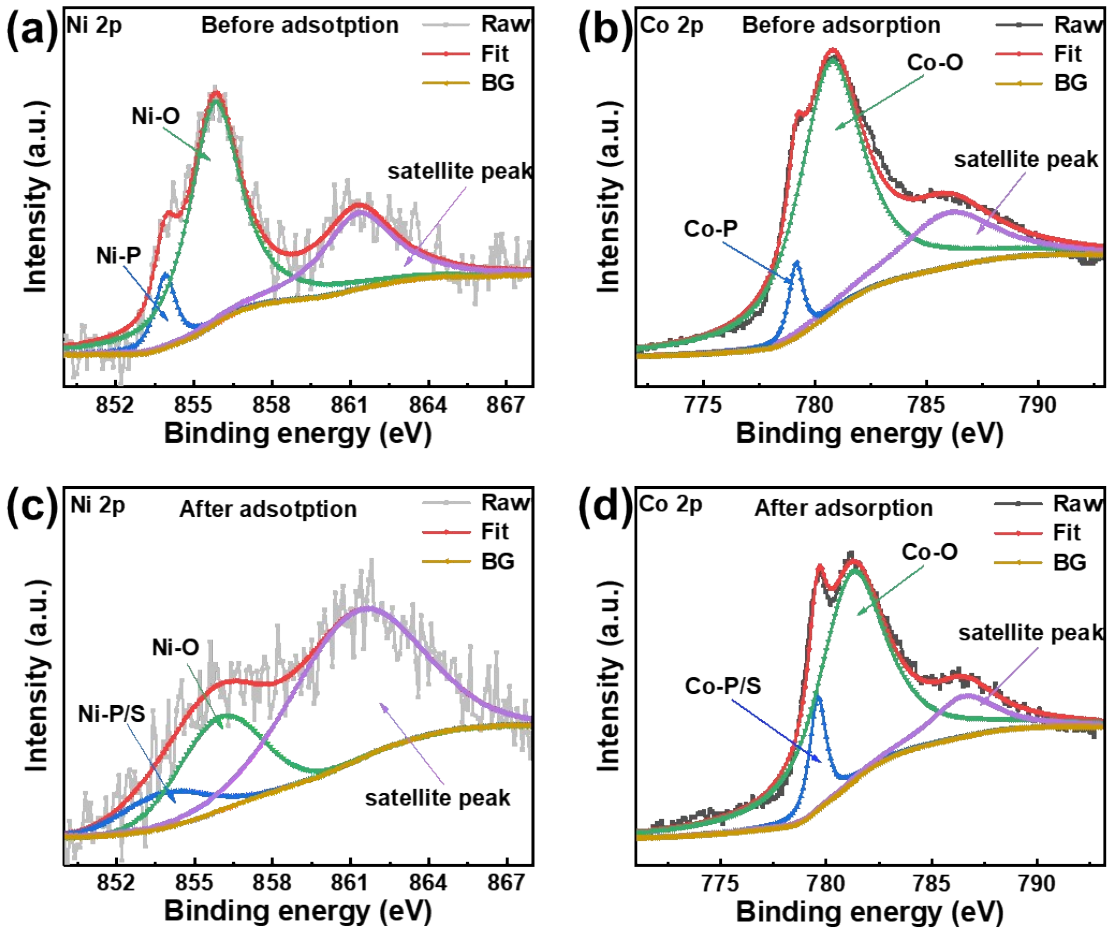

Figure S9. High resolution XPS spectra for the Ni 2p and Co 2p of $NiCo_2P_x$, before and after adsorption of Li_2S_6, where content of O and P in the $NiCo_2P_x$ before adsorption of Li_2S_6 are determined to be 55.33 at% and 9.77 at%, respectively (with a ratio of 5.66: 1).

Sample	XPS peaks	Before adsorption		After adsorption	
		Ni 2p	Co 2p	Ni 2p	Co 2p
$NiCo_2P_x$	0#	0.084	0.048	0.094	0.100
	1#	0.615	0.727	0.249	0.757
$NiCo_2O_4$	0#	0.107	0.396	0.394	0.279
	1#	0.605	0.499	0.361	0.664

Peak 0# refers to the species at low binding energy and peak 1# refers to the ones at medium binding energy in the high resolution spectra.

Table S1. The content of the Ni/Co-contained species in the measured spectra of corresponding samples.

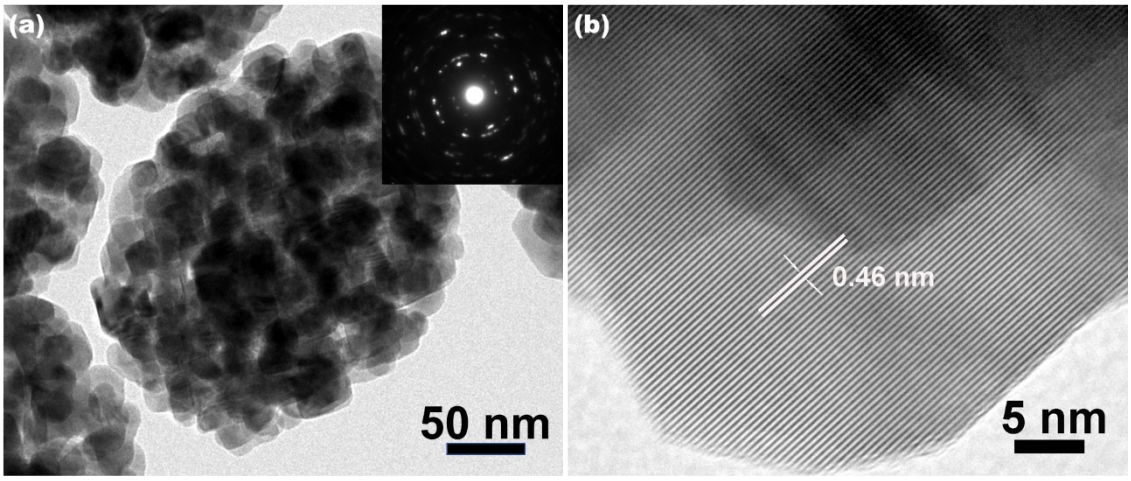

Figure S10. HRTEM image of $NiCo_2O_4$ and its lattice plane (111).

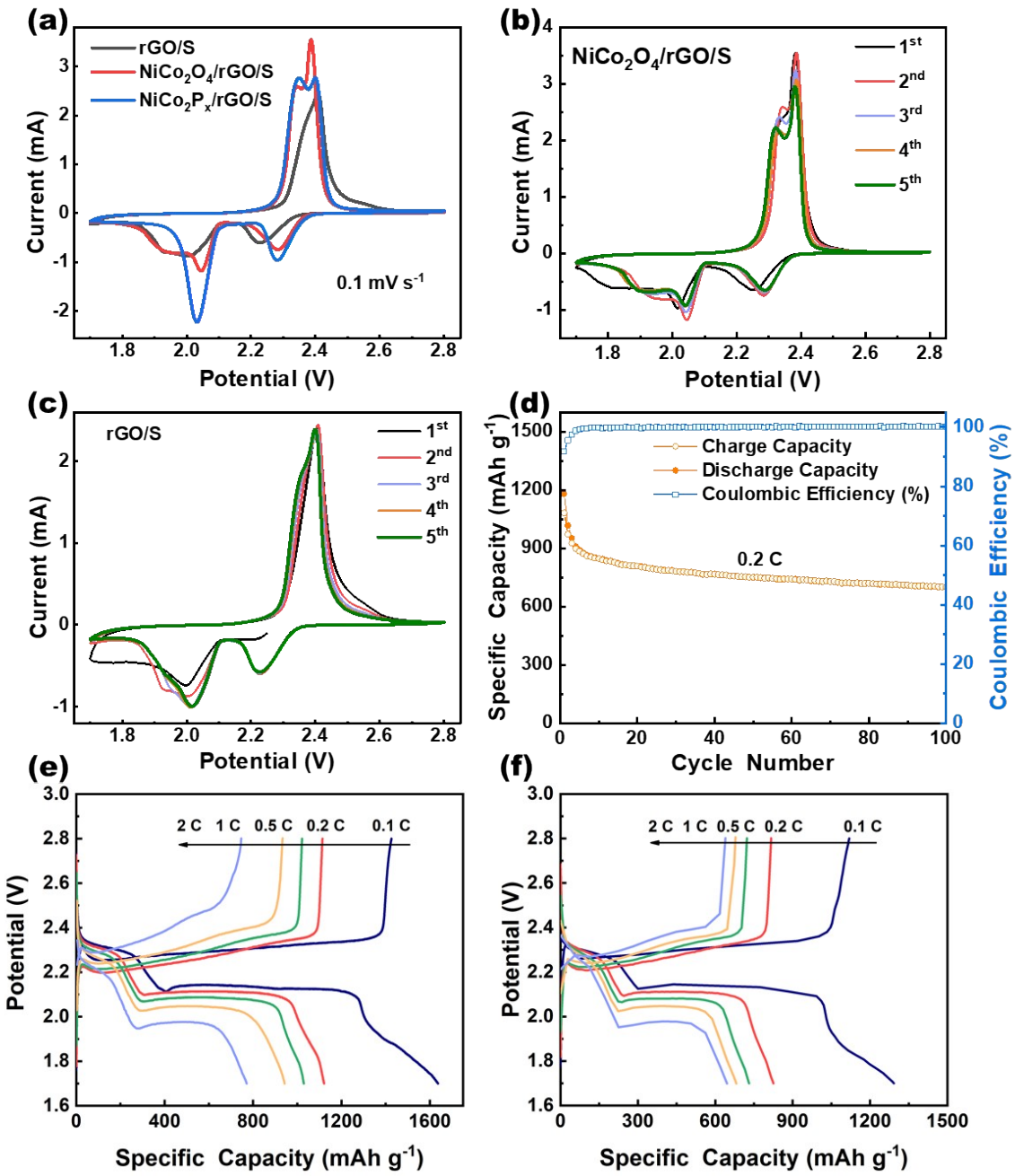

Figure S11. (a) The second cycle of CV curves for $NiCo_2P_x$/rGO/S, $NiCo_2O_4$/rGO/S and rGO/S cathodes; (b) The initial five cycles of CV curves for $NiCo_2O_4$/rGO/S cathode; (c) The initial five cycles of CV curves for rGO/S cathode; (d) Cyclic performance for rGO/S cathode at 0.2 C. (e), (f) Corresponding discharge/charge plots at various current densities for $NiCo_2P_x$/rGO/S, $NiCo_2O_4$/rGO/S, respectively.

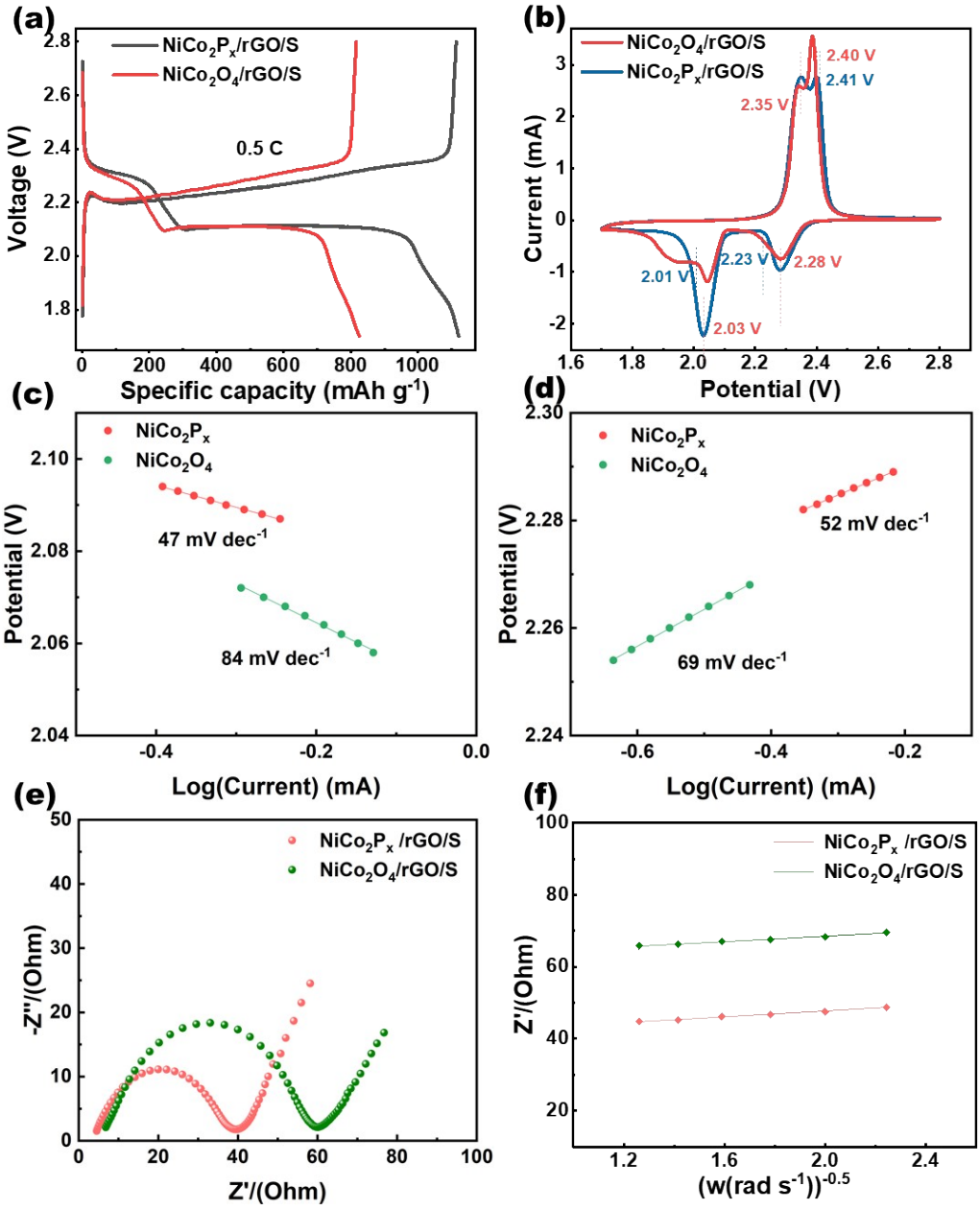

Figure S12. (a) Charge/discharge profiles of the $NiCo_2P_x$/rGO/S and $NiCo_2O_4$/rGO/S electrodes at 0.5 C; (b) The CV curves of 2nd cycle for the $NiCo_2P_x$/rGO/S and $NiCo_2O_4$/rGO/S electrodes at scan rate of 0.1 mV s^{-1}; (c), (d) The Tafel plots derived from (b); (e) EIS spectra of $NiCo_2P_x$/rGO/S and $NiCo_2O_4$/rGO/S electrodes; (f) linear fitting plot of -Z´´ versus $\omega^{-1/2}$.

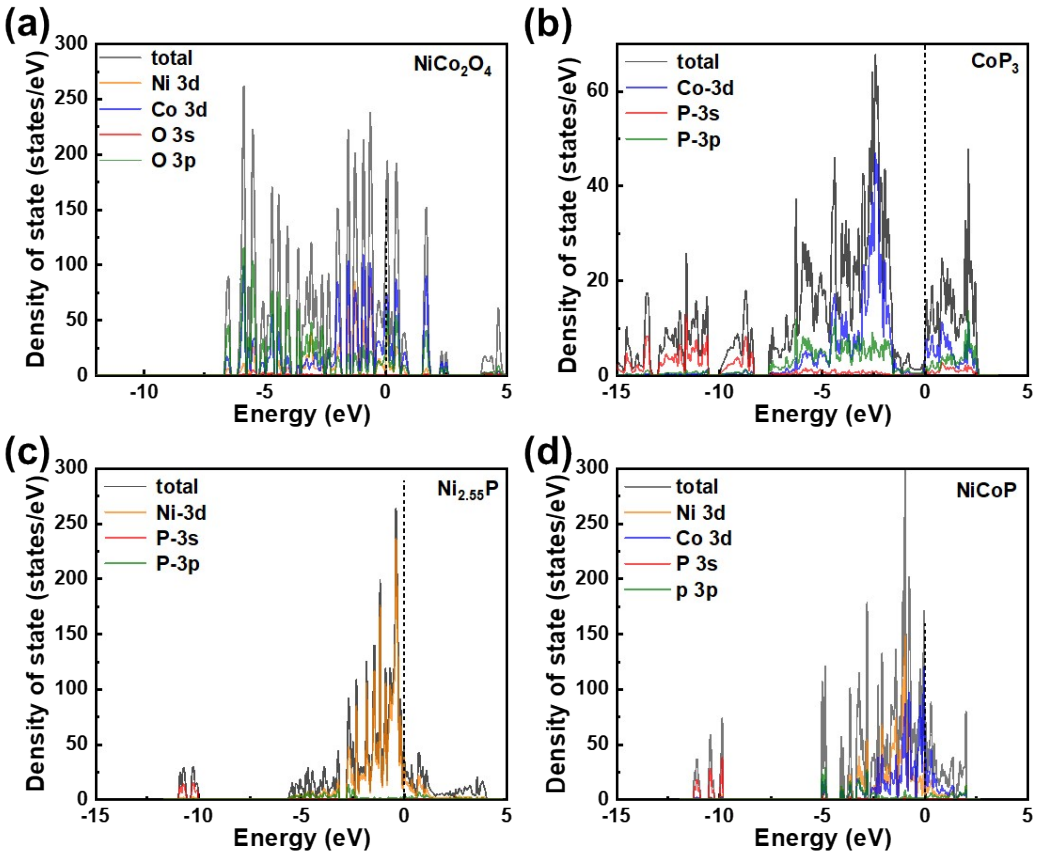

Figure S13. Density of states of (a) $NiCo_2O_4$, (b) CoP_3, (c) $Ni_{2.55}P$ and (d) NiCoP.

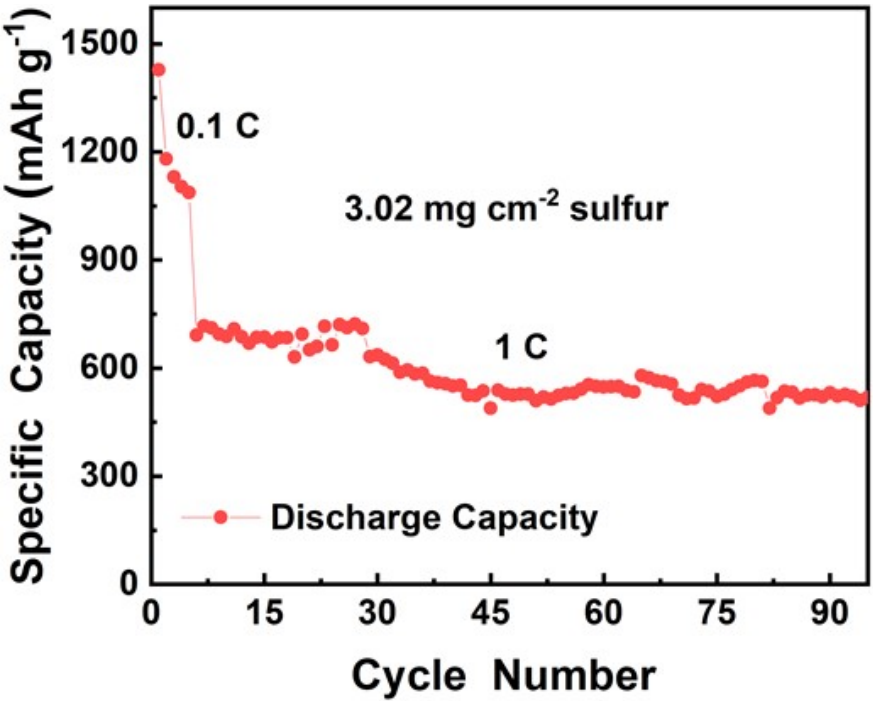

Figure S14. Cycling performance of $NiCo_2P_x$/rGO/S cathode measured at1C upon mass loading of sulfur over 3.0 mg_S cm^{-2} and electrolyte of 10μL mg^{-1}.